

pubs.acs.org/JPCA Article

# Emerging Nonvalence Anion States of [Isoprene-H·]·H₂O Accessed via Detachment of OH-·Isoprene

Marissa A. Dobulis, Michael C. Thompson, Kellyn M. Patros, Thomas Sommerfeld, and Caroline Chick Jarrold\*



Cite This: J. Phys. Chem. A 2020, 124, 2279-2287



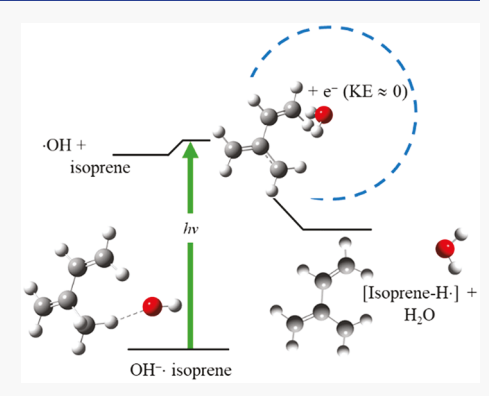
**ACCESS** 

III Metrics & More

Article Recommendations

s Supporting Information

ABSTRACT: The anion photoelectron imaging spectra of an ion with *m/z* 85, generated under ion source conditions that optimize <sup>•</sup>OH production in a coexpansion with isoprene, are presented and analyzed with supporting calculations. A spectroscopic feature observed at a vertical electron detachment energy of 2.45 eV, which dominates the photoelectron spectrum measured at 3.495 eV photon energy, is consistent with the OH⁻-isoprene ion−molecule complex, while additional signal observed at lower electron binding energy can be attributed to other constitutional isomers. However, spectra measured over a 2.2−2.6 eV photon energy range, i.e., from near threshold of the predominant OH⁻-isoprene detachment feature through the vertical detachment energy, exhibit sharp features with common electron kinetic energies, suggesting autodetachment from a temporary anion prepared by photoexcitation. The photon energy independence of the electron kinetic energy of these features along with the low dipole moment predicted for the neutral <sup>•</sup>OH·



isoprene van der Waals complex, suggest a complex photon-driven process. We present calculations supporting a hypothesis that near-threshold production of the \*OH···isoprene reactive complex results in hydrogen abstraction of the isoprene molecule. The newly formed activated complex anion supports a dipole bound state that temporarily traps the near zero-kinetic energy electron and then autodetaches, encoding the low-frequency modes of the dehydrogenated neutral isoprene radical in the electron kinetic energies.

## ■ INTRODUCTION

Isoprene (2-methyl-1,3-butadiene) comprises about half of total biogenic nonmethane volatile organic compound emissions globally each year. Oxidation of isoprene by the hydroxyl radical, the latter of which is often referred to as a detergent of the atmosphere because it is the primary agent for removal of atmospheric volatile organic compounds (VOCs), initiates a series of reactions that results in tropospheric ozone formation and OH propagation. The oxidation of isoprene in particular involves OH addition to one of the four sp² hybridized carbon centers along the butadiene backbone. Hydrogen (H) abstraction by OH is a higher barrier reaction than OH–VOC adduct formation for unsaturated VOCs, 10-23 though abstraction pathways have been suggested for several substituted allylic species to occur from nearly atmospheric to combustion-like temperatures, as well as very low pressures.

While a plethora of kinetic<sup>5,12</sup> and computational<sup>13,14,17,28</sup> studies on OH + VOC reactions have been reported in the literature, there have been a few spectroscopic studies on products of either hydroxyl addition or hydrogen (H) abstraction.<sup>29</sup> In an effort to glean more detailed structural information on the neutral radical OH—isoprene reaction complex, we present the anion photoelectron (PE) spectrum of

the closed-shell anion, similarly to those previously reported for other neutral radical species with closed-shell anions. <sup>30–32</sup> As will be described below, the most intense feature observed in the spectrum is consistent with the OH<sup>-</sup>-isoprene ion—molecule complex (IMC), while additional, lower intensity features are attributed to constitutional isomers of this complex. Interestingly, spectra measured with photon energies near the threshold of the OH<sup>-</sup>-isoprene IMC detachment transition exhibit autodetachment features that suggest a more complex photochemical process is taking place.

## METHODS

The anion PE imaging apparatus used in this study has been described previously. <sup>33</sup> Ions were generated by coexpanding a mixture of 27.5%  $\rm H_2$ , ~2%  $\rm O_2$ , ~1% isoprene, and balance  $\rm Ar^{34}$  (60 psig) using a pulsed molecular beam valve through a needle electrical discharge, <sup>35</sup> which was stabilized by a hot,

Received: February 13, 2020 Published: February 24, 2020



biased thoriated iridium ribbon electron emitter. The H<sub>2</sub>/O<sub>2</sub> mixture produces significant quantities of OH and OH in the discharge source. After expansion, the gas mixture passed through a skimmer, and the anions were accelerated to 1 keV into a time-of-flight mass spectrometer.<sup>36–38</sup> Anions of interest were selectively photodetached using a range of photon energies from a tunable optical parametric oscillator (Ekspla NT 342) and the second harmonic (532 nm, 2.330 eV) and third harmonic (355 nm, 3.495 eV) outputs of a Nd:YAG laser (Continuum Surelite, 30 Hz). Photoelectron kinetic energies (e<sup>-</sup>KE) were measured using velocity map imaging.<sup>39,40</sup> Threedimensional PE velocity distributions were obtained from the resulting image using BASEX<sup>41</sup> and then converted to e<sup>-</sup>KE by calibration with the PE image of O<sub>2</sub><sup>-.42</sup> PE spectra shown below are primarily plotted as a function of electron binding energy,  $e^{-}BE = h\nu - e^{-}KE$ , which is independent of photon energy.

Discharge-based ion sources can produce a broad range of species, and a typical mass spectrum of species in the m/z range 60–105 generated using this particular gas mixture (vide supra) is shown in Figure 1. The singly charged complex anion

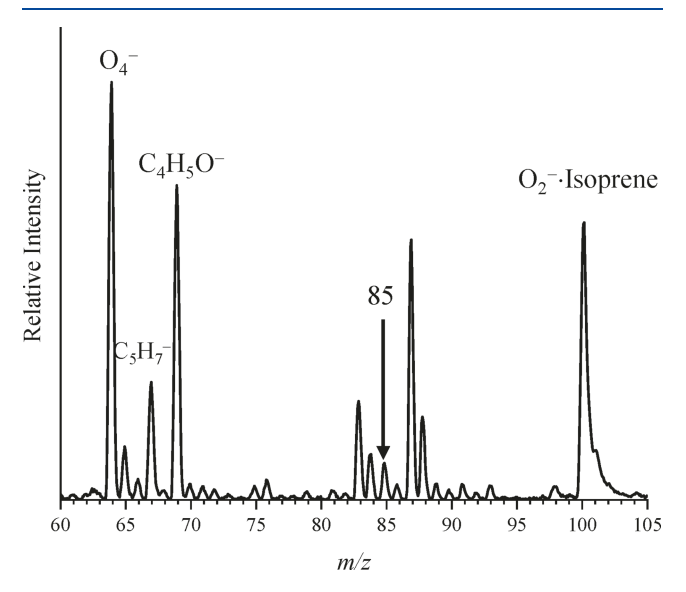


**Figure 1.** Typical mass spectrum of the mix of hydrogen, oxygen, argon, and isoprene showing  $60 \le m/z \le 105$ . The m/z value coinciding with OH–isoprene species is 85, indicated by the arrow. Several other ions that have been identified unambiguously are labeled.

formed between  ${}^{\bullet}$ OH and isoprene is m/z 85. However, this general C<sub>5</sub>H<sub>9</sub>O<sup>-</sup> m/z 85 could assume many different molecular structures, and the m/z 85 peak could also be attributed to C<sub>7</sub>H<sup>-</sup>, C<sub>4</sub>H<sub>5</sub>O<sub>2</sub><sup>-</sup>, and C<sub>3</sub>HO<sub>3</sub><sup>-</sup>. On the basis of the absence of other  $C_nH^ (n \neq 7)$  clusters and trioxygenated species in the mass spectrum, we conclude that C<sub>7</sub>H<sup>-</sup> and  $C_3HO_3^-$  are not significantly populating the m/z 85 ion packet. However, to determine whether multiple structures with C<sub>5</sub>H<sub>9</sub>O<sup>-</sup> and C<sub>4</sub>H<sub>5</sub>O<sub>2</sub><sup>-</sup> molecular formulas may be populating the ion beam, we turned to computational results on the constitutional isomers of C<sub>5</sub>H<sub>9</sub>O<sup>-</sup>/C<sub>5</sub>H<sub>9</sub>O, including the OH-isoprene IMC/OH-isoprene van der Waals complex, various possible alkenoxide/alkenoxy species, the molecular ion (MI) and neutral of the HO-isoprene radical adducts,  $HO-Cx^{-}/HO-Cx$  (x indexing the C atom on the butadiene backbone), and the H-abstracted isoprene-water [IsopreneH] $^-\cdot H_2O$ /[Isoprene- $H^{\bullet}$ ] $\cdot H_2O$  complexes. Also considered were the constitutional isomers of  $C_4H_5O_2^-$ , including various possible butadiene-based peroxide anions, various diketone and aldehyde-ketone species, and conjugate base species, along with corresponding neutral species.

Molecular structures of each species of interest were optimized via MP2/ma-def2-TZVP(-f). 43,44 These were followed by single-point calculations at the domain-based local pair-natural orbital-based singles and doubles coupled cluster including noniterative triples excitations [DLPNO-CCSD(T)] level of theory with the aug-cc-pVTZ basis set for the anions 45-48 for a comparison of total energies, and ionization potential equation-of-motion singles and doubles coupled cluster level of theory (IP-EOM-CCSD/aug-cc-pVTZ) for vertical detachment energies (VDEs). 49,50 These VDE values can be compared to the energy at which the highest intensity detachment transition appears in the experimental spectra in order to identify species present.

Adiabatic detachment energies (ADEs), the energy difference between the zero-point levels of an anion and the lowest energy minimum on the potential energies surface of the corresponding neutral, were computed for a smaller subset of the possible structures via orbital-optimized MP2 (OO-MP2/ ma-def2-TZVP(-f)). Orbital-optimized MP2 is needed because, for various neutral doublets, spin contamination is rather large ( $\langle S^2 \rangle$  up to 1.5) if unrestricted Hartree-Fock-based wave functions are employed, but very small ( $\langle S^2 \rangle$  less than 0.77) with OO-MP2. Furthermore, for a few IMCs, the larger aug-ccpVTZ basis set was studied, and an alternative protocol was considered, where the ADE is computed as the sum of the distortion energy of the anion (to the geometry of the neutral) and the VDE (obtained with IP-EOM-CCSD), so that no spincontamination influences the ADE via the geometry optimization of the neutral. Two more sophisticated protocols bracket the OO-MP2/ma-def2-TZVP(-f) ADE by about  $\pm 0.25$ eV, and we conclude that OO-MP2/ma-def2-TZVP(-f) represents a well-balanced cost-efficient approach. Version 4.1.2 of the ORCA package, 51,52 was used for all ab initio calculations.

For comparison, we additionally performed density functional theory (DFT) calculations for the ADEs and VDEs of various species using dispersion-corrected Coulomb attenuating method Becke three-parameter, Lee, Yang, and Parr (CAM-B3LYP) $^{53}$  functional with the aug-cc-pVTZ basis set. These calculations were completed using the Gaussian  $09^{54}$  and  $16^{55}$  suites.

Lastly, we performed an extensive search for species or conformations that may support a dipole-bound state (DBS), or, more generally, a nonvalence bound state. For all optimizations of neutrals, OO-MP2/ma-def2-TZVP(-f) was used for the reasons stated above. At any given geometry, the existence of DBSs was studied using excited-state EOM-CCSD (EE-EOM-CCSD), and IP-EOM-CCSD: The binding energy of all excited bound anion states is obtained as a difference between the VDE and the excitation energies. For the DBS calculations the aug-cc-pVDZ basis set used was extended with a (6s6p3d) set of diffuse functions (even-scaled exponents, even-scaling factor 4). This set was placed on an atom or a ghost center close to the positive end of the polarity-causing group of the respective molecule, e.g., the H atom of the OH in OH-isoprene complexes, the O atom of the water molecule in [Isoprene-H<sup>•</sup>]·H<sub>2</sub>O complexes, or the C atom attached to the peroxyl group in peroxides.

Table 1. Summary of Lowest Energy Conformer C<sub>5</sub>H<sub>9</sub>O Computational Results<sup>a</sup>

	relative energy		VDE
potential C <sub>5</sub> H <sub>9</sub> O <sup>-</sup> isomers	MP2/ma-def2-TZVP(-f) (eV)	DLPNO-CCSD(T)/aug-cc-pVTZ (eV)	IP-EOM-CCSD/aug-cc-pVTZ (eV)
separated OH <sup>-</sup> + isoprene	0.00	0.00	N/A
molecular ions of OH-isoprene adducts			
HO-C1	-0.62	N/A	0.85
HO-C2	-0.17	N/A	N/A
HO-C3	-0.13	N/A	1.16
HO-C4 <sup>-</sup>	-0.59	-0.47	0.77
OH-isoprene ion-molecule complexes			
C1/methyl pocket	-0.65	-0.63	2.64
C1/C3 pocket	-0.65	-0.63	2.66
C4 hydrogen bond	-0.51	-0.49	2.52
C4/methyl pocket	-0.67	-0.66	2.70
$[Isoprene-H]^- \cdot H_2O$	-0.69	-0.64	1.37
alkenoxides			
O <sup>-</sup> -C1	-0.89	N/A	2.08
O <sup>-</sup> -C2	-1.16	N/A	2.13
O <sup>-</sup> -C3	-1.94	N/A	1.49
O <sup>-</sup> -C4	-0.99	N/A	2.09

<sup>&</sup>lt;sup>a</sup>Lowest relative energy species are bolded. Structures were optimized using MP2/ma-def2-TZVP, followed by single-point DLPNO-CCSD(T)/aug-cc-pVTZ calculations. Vertical detachment energies (VDEs) were calculated at IP-EOM-CCSD/aug-cc-pVTZ using the optimized anion structure.

## ■ RESULTS AND DISCUSSION

Figure 2 shows PE spectra of the m/z 85 ion obtained with 2.330 eV (green trace), 2.883 eV (blue trace), and 3.495 eV (purple trace) photon energies. The spectra measured with 3.495 and 2.883 eV photon energies are dominated by a feature labeled X with VDE =  $2.45 \pm 0.02$  eV. From the 2.883 eV spectrum, which exhibits a  $1060 \pm 20 \text{ cm}^{-1}$  shoulder progression on the high e<sup>-</sup>BE falling edge, we approximate the adiabatic detachment energy of band X to be  $2.33 \pm 0.05$  eV. Therefore, the spectrum measured with 2.330 eV photon energy (green trace) is near the threshold for this transition. All spectra show two broader and less intense features to lower e<sup>-</sup>BE values. The lower e<sup>-</sup>BE features, labeled x' and x", have approximate origins at  $1.1 \pm 0.1$  and  $1.75 \pm 0.05$  eV, respectively. Band x" has a distinct VDE of 1.87 eV in the 2.330 eV spectrum. Finally, the spectrum measured using 3.495 eV exhibits three peaks spaced by 890 cm<sup>-1</sup> at 2.79, 2.90, and 3.01 (±0.04) eV, labeled A. There is also a platform of continuum signal from 2.7 to 3.495 eV in this spectrum, which is not observed above 2.7 eV in the 2.883 eV spectrum.

We first consider the assignment of band X, incorporating the results of calculations on the various  $C_5H_9O^-$  constitutional isomers, summarized in Table 1. They predict the following: (1) The alkenoxides, which can form by -H shift in the OH-isoprene adduct MI, are lowest in energy but generally have VDE values in the range 1.49-2.13 eV, below the observed 2.45 eV VDE. We note here that calculated VDEs are not corrected for zero-point energies, which results in a slight systematic overestimation of the value. (2) The OH-isoprene and [Isoprene-H]<sup>-</sup>·H<sub>2</sub>O IMCs are nearly isoenergetic and are predicted to be 0.2-0.4 eV higher in energy than the least stable alkenoxide. However, the calculated VDEs of the OH-isoprene IMCs, which range from 2.52 to 2.7 eV depending on the conformer, are in close agreement with the observed spectrum, particularly considering the previously noted expected overestimation. In contrast, the [Isoprene-H]-H<sub>2</sub>O IMC has a calculated VDE of 1.37 eV. (3) The HOisoprene adduct MIs,  $HO-Cx^-$ , are predicted to be 0.1-0.5

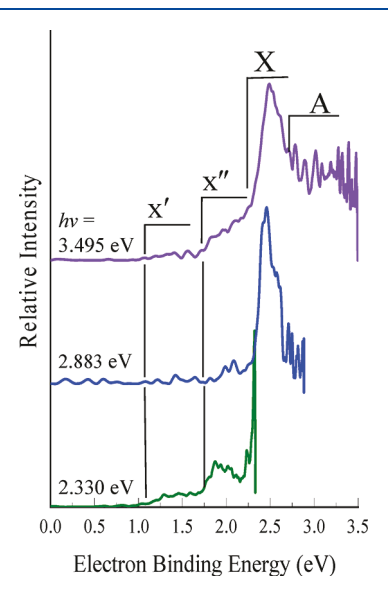


Figure 2. PE spectra of the m/z 85 anions at 3.495 eV (violet), 2.883 eV (blue), and 2.330 eV (green) photon energies.

eV higher in energy than the IMCs and have calculated VDE values closer to 1 eV. Results of DFT calculations are in qualitative agreement with these results. The VDE values calculated at the CAM-B3LYP level for the adduct MIs and the OH $^-$ isoprene IMC were marginally higher than those calculated at the IP-EOM-CCSD/aug-cc-pVTZ level, while the values calculated via DFT for the alkenoxide species were marginally lower than those at the IP-EOM/CCSD/aug-cc-pVTZ level.

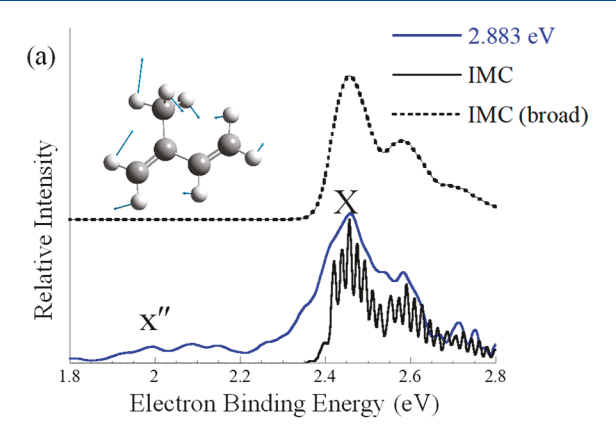
Within the  $C_4H_5O_2$  family, the computational results, which are included in the Supporting Information, predict several peroxide species having VDEs comparable to what was observed. However, the associated ADE – VDE differences (calculated at CAM-B3LYP/aug-cc-pVTZ) suggest much broader transitions than what is observed. The conjugate base anions of the carboxylic acid isomers, which seem less

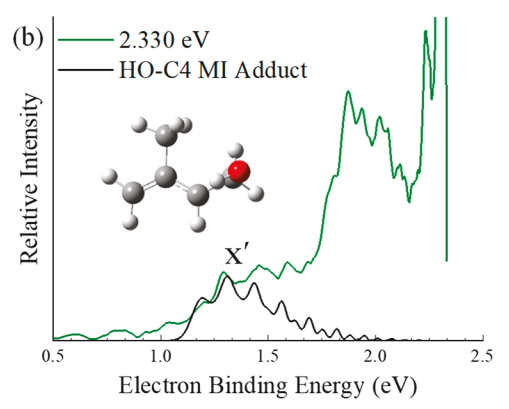
likely to form given the extensive structural rearrangement leading to their formation from the starting materials present in the ion source, are predicted to have VDE values of ca. 3.8 eV. Dicarbonyl structures, which would also require significant structural rearrangement, were also predicted to have higher-than-observed VDE values.

We therefore assign band X to the OH<sup>-</sup>·isoprene IMC. Simulations using spectroscopic parameters calculated from the DFT-optimized IMC and van der Waals complexes were not practical using our own simulation code, 56 which invokes a number of approximations that are valid only for rigid molecules. For the present species, there is a very large difference in intermolecular distances between the two charge states and the change in orientation of the OH relative to isoprene for this system, which makes the assumption of a rigid molecule problematic. As a first-order treatment of the system, we approximated simulation parameters on the basis of the difference between the ADE and VDE values, 0.18 eV. The \*OH-isoprene intermolecular potential is relatively flat: The Franck-Condon overlap between the IMC and the zero-point state of the neutral complex is vanishingly small, while maximum overlap will be with a neutral complex on a modestly repulsive part of the neutral potential. Therefore, the 0.18 eV spread between the ADE and VDE values can be taken as an approximate lower limit of the repulsion energy on the neutral surface with the largest Franck-Condon overlap with the IMC. Our simulation is based on CAM-B3LYP/aug-ccpVTZ optimizations of the complex in which the \*OH/OH is situated in the methyl-C4 pocket (Supporting Information), coupled with incorporating excitation of isoprene-local modes based on the relative structures of the isoprene in the IMC and free isoprene. A simulation that has been broadened to account for accessing a dissociative portion of the intermolecular potential is shown in Figure 3a, along with an unbroadened simulated spectrum superimposed on the experimental spectrum obtained with 2.883 eV. The simulation does show a 1021 cm<sup>-1</sup> vibrational shoulder progression similar to that of the observed spectrum. This isoprene-local mode is shown in the inset of Figure 3a. This mode is active because of the reduction in strength of the nontraditional H-bonding [C-H···-OH] upon photodetachment. Also active are unresolved low-frequency vibrational modes of the butadiene backbone of the IMC, which is slightly nonplanar in the anion. The origin of this simulation was set at 2.40 eV, though this value should be taken as an upper limit on the ADE, given very low Franck-Condon overlap between the zero-point levels of the strongly bound IMC and weakly bound van der Waals complex. We acknowledge that other conformers likely contribute to the broadness of this feature with similar vibrations.

The EA of  ${}^{\bullet}\text{OH}$  is 1.8277 eV,  ${}^{57,58}$  putting an upper limit on the OH $^-$  + isoprene solvation energy at 0.574 eV. This value is comparable to the 0.6 eV solvation energy determined from the PE spectrum of  ${\rm O_2}^-$ -isoprene. We note that the OH $^-$ CH $_4$  shift reported by Continetti and co-workers is 0.27 eV; methane is less polarizable and lacks the OH $^-$  encompassing pocket available in isoprene, and  ${\rm C(sp^2)-H}$  bonds are more polar than  ${\rm C(sp^3)-H}$  bonds, further enhancing the charge stabilization.

The lower intensity features observed at lower e $^-BE$ , bands x' and x'', do exhibit VDEs that are consistent with what would presumably be an ensemble of the HO $^-$ isoprene adduct MIs (VDEs range from 0.77 to 1.16 eV) and the alkenoxides (VDEs range from 1.4 to 2.1 eV). The HO $^-$ C4 adduct MI





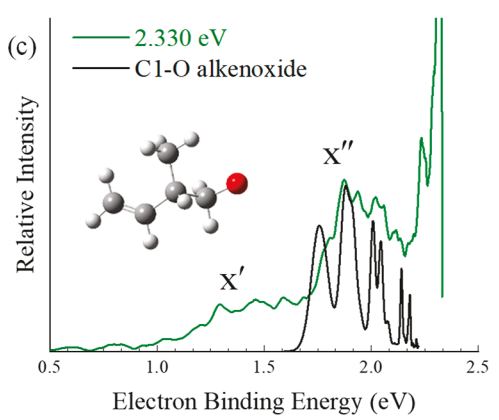


**Figure 3.** Franck—Condon simulations of (a) OH<sup>−</sup>·isoprene IMC, (b) HO−C4 adduct MI, and (c) C1−O alkenoxide species formed by −H transfer. Simulation parameters are in the Supporting Information.

simulation in Figure 3b serves as a representation of what could be several overlapping  $HO-Cx^-$  spectra. Simulation parameters are available in the Supporting Information. The representative  $HO-Cx^-$  structure is inset in Figure 3b. Finally, we note that band x'' shows a profile and binding energy comparable to the alkenoxides studied previously.<sup>32</sup> The simulation of a representative alkenoxide spectrum, with oxygen addition to C1 [inset in Figure 3c], is shown superimposed on the 2.330 eV spectrum of m/z 85 in Figure 3c. Again, we assume that there would be an ensemble of m/z 85 alkenoxides contributing to this portion of the spectrum, and the single simulation is shown as a representative of the other potential species present.

Having assigned the major transitions in the spectrum, we now consider the near-threshold signal observed in the PE

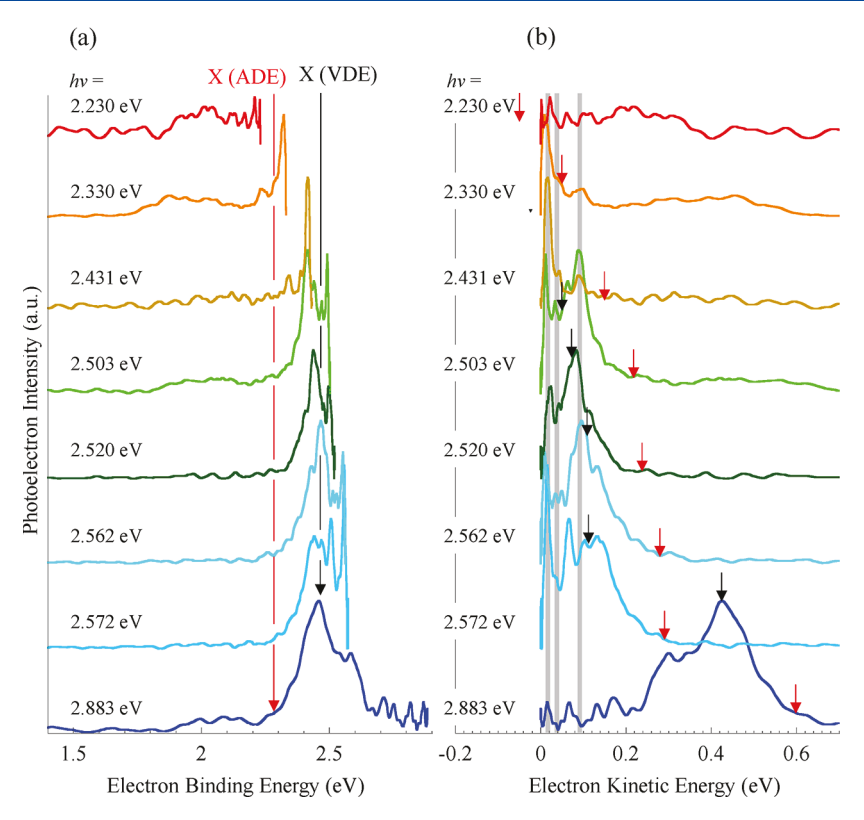


Figure 4. PE spectra over a range of photon energies as plotted as a function of (a) e<sup>-</sup>BE and (b) e<sup>-</sup>KE. Approximate origins for band X are shown with the red arrow and the approximate VDE is shown by the black arrows in both panels. Gray lines highlight the common e<sup>-</sup>KE features seen in multiple spectra in panel b.

spectrum measured using 2.330 eV photon energy (Figure 2). This spectrum exhibits a reproducible, intense, near-threshold feature at  $e^{-}KE = 120 \pm 7 \text{ cm}^{-1}$ , with a less intense shoulder at  $e^{-}KE = 370 \pm 10 \text{ cm}^{-1}$  and peak at  $e^{-}KE = 725 \pm 10 \text{ cm}^{-1}$ . These would correspond to e-BE values of 2.315, 2.284, and 2.24 eV, respectively. However, these features remain at constant e KE as the photon energy is tuned through the threshold, as shown in Figure 4. For example, the PE spectrum measured with 2.431 eV photon energy (510 nm), shown as the mustard trace, exhibits peaks at identical e-KE values and relative intensities, as can be seen when plotted against e KE [Figure 4b] rather than eBE [Figure 4a]. To guide the eye, the approximate ADE is indicated by the red arrows, and the VDE is indicated by the black arrows in Figure 4a,b. Note that the lowest photon energy (2.230 eV) used falls below the approximate ADE. Spectra measured with incrementally higher photon energies than 2.431 eV also exhibit this e<sup>-</sup>KE = 120 cm<sup>-1</sup> peak, with the other peaks increasing in relative intensity with increasing photon energy. Additionally, a peak at e<sup>-</sup>KE =  $530 \pm 10$  cm<sup>-1</sup> is prominent in the spectrum collected with 2.572 eV photon energy. The direct detachment signal associated with band X becomes more apparent at higher photon energies. These sharp features at low e-KE are not distinguishable from the noise in the spectra measured with 2.883 or 2.230 eV photon energies.

Enhancement of transitions to certain vibrational levels in photodetachment can occur when the photon energy happens to be resonant with a quasibound vibrational level of an anion state, which then undergoes vibrational autodetachment in addition to direct detachment to the (enhanced) final neutral level. This phenomenon is not unusual in neutrals with large dipole or quadrupole moments or can otherwise support an

electron in a nonvalence bound state near the detachment continuum, as those reported by Mabbs, <sup>59,61</sup> Wang, <sup>62,64</sup> Bowen, <sup>65,66</sup> and Lineberger. However, according to our calculations, the neutral OH-isoprene van der Waals complex does not support a nonvalence bound state. This negative result is astonishing insofar as the conditions for the support of a nonvalence bound state are favorable: The neutral complex possesses first a dipole moment of 2.4 D, equal or close to the range (2.4 D<sup>72</sup> to 2.5 D<sup>73</sup>) normally considered critical for actual molecules; second, a fairly substantial polarizability; and, third, the vertical product with the greatest Franck-Condon overlap has a small excluded volume, as the dipole essentially originates from the OH bond, and in the anion the H atom is pointing away from the isoprene moiety. "Excluded volume" is any volume near the positive center of the dipole of the neutral that is taken up by nonpolar groups or substituents so that the excess electron cannot occupy it. <sup>74</sup> We note that finite basis set computations can never exclude the presence of extremely diffuse states, but we are confident to rule out states with binding energies in excess of 2 cm<sup>-1</sup>. In addition, the features shown in Figure 4 are different from those typically observed in the case of an excited anion state near the detachment continuum. These features are more akin to the O2vibrational autodetachment observed in  $O_3^-$  ( $O_2$ )<sub>n</sub> clusters, <sup>33</sup> in which photodissociation of ozonide in the cluster produced vibrationally excited O2- fragments that underwent autodetachment that encoded the  $O_2^-$  vibrational frequency rather than ozonide vibrational frequencies. O2- vibrational autodetachment has also been previously observed in electron attachment to ozone.<sup>75</sup>

We consider the neutral + e<sup>-</sup> system prepared by the nearthreshold detachment of the OH<sup>-</sup>-isoprene IMC. Figure 5

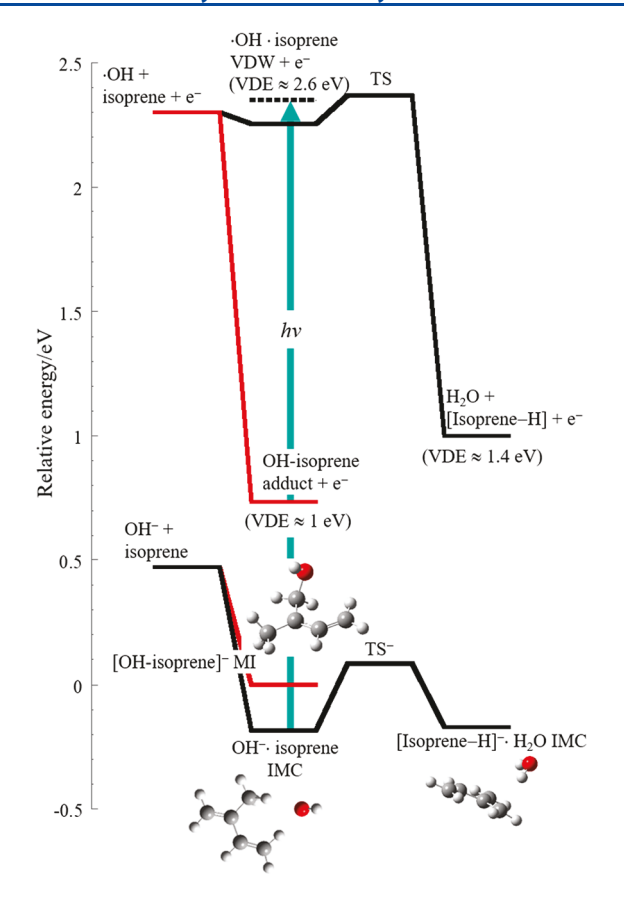


**Figure 5.** Relative energies of the OH<sup>-</sup>isoprene IMC, the  $HO-Cx^-$  MI, and the [Isoprene-H]<sup>-</sup>·H<sub>2</sub>O IMC, with corresponding neutrals. TS and TS<sup>-</sup> refer to the transition states for H-abstraction on the anion and neutral surfaces, respectively.

shows relative energies of the anion and neutral IMC and van der Waals complex, along with the various species that fall within the energy between these two limits. Note that for all species, there are multiple conformers with relative energies that vary by tenths of an electronvolt, so the energies shown are approximate. In the case of threshold detachment of the lower energy OH<sup>-</sup>-isoprene IMC conformers, a neutral \*OH radical is prepared with the O-center in the pocket between the allylic and methyl H atoms. This structure is different from the optimized neutral van der Waals complexes, in which the \*OH is orthogonal to the plane of the butadiene backbone with the O-center pointing toward the more positive C2 or C3 atoms.<sup>28</sup>

Before a hypothesis regarding the nature of the autodetaching state can be put forward, a structure that supports a DBS (or nonvalence bound state) must be identified. We considered a variety of geometries, but from a formation kinetics point of view, the most likely candidates are  ${}^{\bullet}$ OH-isoprene and [Isoprene-H ${}^{\bullet}$ ]·H<sub>2</sub>O. We also consider peroxy radicals with the formula  ${}^{\bullet}$ O<sub>2</sub>-C<sub>4</sub>H<sub>5</sub>. Our results can be summarized as follows:

- 1. Peroxy radicals show the largest dipole moments (up to 3.8 D) compared to the other hypothetical structures. Nonetheless, peroxy radicals do not support any DBS, presumably owing to their excluded volume.
- OH-isoprene structures possess dipoles at the lower end of the range considered critical in real molecules (2.4-2.5 D) as well as substantial polarizabilities and

small excluded volumes; however, EOM-CCSD calculations nevertheless fail to identify any DBS.

3. [Isoprene-H<sup>•</sup>]·H<sub>2</sub>O forms two types of conformers. In the lower energy conformers, the H<sub>2</sub>O is in an axial position above the [Isoprene-H<sup>•</sup>] plane, and the two OH bonds point toward the π-system. The dipole is again on the order of 2.4 D, and we are unable to find any DBSs. As the OH bonds point toward the [Isoprene-H<sup>•</sup>] moiety, the excluded volume effect is large and the absence of DBSs is not surprising.

In the second type of conformer, the  $H_2O$  molecule lies in an equatorial position in the [Isoprene- $H^{\bullet}$ ] plane, and the two OH bonds point away from the [Isoprene- $H^{\bullet}$ ] moiety. These structures lie 40–60 meV higher in energy than the first conformer class. The dipoles of the second type of conformer are slightly larger (up to 2.5 D), but more importantly, the excluded volume is very small, and our calculations indicate the existence of DBSs with binding energies between 5 and 20 cm<sup>-1</sup>. A representation of the isosurface containing 60% of the electron density of the singly occupied dipole-bound orbital of such a conformer is shown in Figure 6.

In view of these results we hypothesize that the observed autodetaching state corresponds to vibrationally excited levels of a ([Isoprene-H $^{\bullet}$ ]·H<sub>2</sub>O)<sup>-</sup> DBS. This structure can be formed by excitation of an OH-isoprene where the OH- is in one of the pockets adjacent to the methyl group. From this geometry, the rearrangement to an [Isoprene-H•]·H<sub>2</sub>O structure is essentially a hydrogen shift plus modest relaxations. If the excitation of OH-isoprene happens very close to threshold, the energy of the outgoing electron is near zero, and it may be caught into the DBS during the H-shift. The H-shift, which originates from the vertical geometry reached by excitation, is found to be a barrierless downhill process and can be thought to happen fast. Unique, nonlocal properties have been observed in combination with breakdown of the Born-Oppenheimer approximation near threshold in a variety of diatomics 76,77 and potentially along select modes in polyatomics.<sup>78</sup>

The autodetachment features with common e-KE observed over a range of photon energies between 2.3 and 2.6 eV point to photon-driven production of a vibrationally excited species that is chemically different from the initial anion state over this energy range, as noted above. In this case, low-frequency modes of the transition state complex are encoded in the e<sup>-</sup>KE's of the autodetached electrons. Assuming the  $\Delta v = -1$ propensity rule for vibrational autodetachment, \$59-71 the e-KE values encode the vibrational spacings of various modes in the DBS, which in general are nearly identical to those of the neutral, minus the binding energy of the DBS. The initially planar butadiene backbone is slightly buckled in the neutral [Isoprene-H•] radical, suggesting the vibrational modes involve the low-frequency backbone bend modes. The [Isoprene-H<sup>•</sup>] radical has 30 vibrational modes (39 for the [Isoprene-H•]·H<sub>2</sub>O complex), with a number of low-frequency modes that can be described as backbone bends and twists. Table 2 summarizes four such modes with DFT calculated unscaled harmonic vibrational level spacings that are ca. tens of cm<sup>-1</sup> higher than the observed e<sup>-</sup>KE values (120, 370, 530, and 725 cm<sup>-1</sup>), which would be consistent with  $\Delta v = -1$ vibrational autodetachment of the DBS.

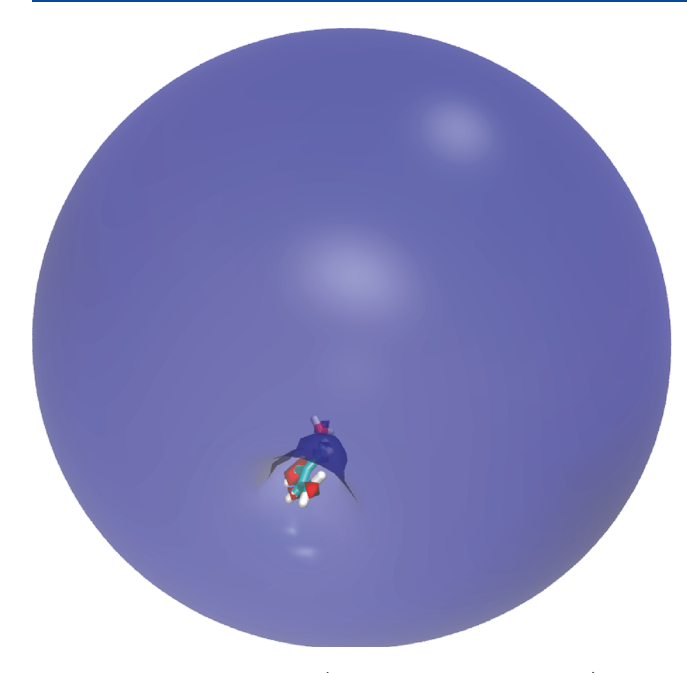


**Figure 6.** "Singly occupied" (occupation number 0.9996) EOM-CCSD natural orbital describing the dipole-bound electron for one conformer of the [Isoprene— $H^{\bullet}$ ]· $H_2O$  complex with an equatorial water. The isosurface shown encloses 60% electron probability density.

Table 2. Four of the 30 Harmonic Unscaled Vibrational Frequencies Resulting from CAM-B3LYP Calculations on the Neutral [Isoprene-H\*] Radical That May Be Implicated in Vibrational Autodetachment of the ([Isoprene-H]·H<sub>2</sub>O)<sup>-</sup>DBS

mode	calc freq/cm <sup>-1</sup>	exp eKE/cm <sup>-1</sup>
backbone twist	136	120
backbone distortion	386	370
backbone distortion	537	530
C4-C <sub>methyl</sub> twist	760	730

Finally, we comment on band A observed in the 3.495 eV spectrum, but not in the 2.883 eV photon energy spectrum shown in Figure 2. This band consists of a progression of narrow features that fall between e<sup>-</sup>KE values of 0.49 and 0.80 eV. We observed a similar, though subtle, enhancement of signal in the O<sub>2</sub>-isoprene spectrum in this e<sup>-</sup>KE range.<sup>30</sup> A much more dramatic enhancement was observed in the PE spectrum of O<sub>2</sub>-benzene, which we attributed to a resonance with a temporary anion state of benzene<sup>30</sup> on the basis of both the energy and the vibrational progression that matched a progression observed in electron transmission studies on benzene. <sup>79</sup> In the case of OH<sup>-</sup>-isoprene, these features appear in an e-KE window similar to the temporary anion state observed for butadiene.<sup>79</sup> We therefore tentatively assign band A to a resonance with the temporary \*OH·[isoprene] state. Further studies on this system are underway.

# CONCLUSIONS

To summarize, the anion PE spectrum of the m/z 85 ion generated by coexpanding isoprene,  $O_2$ , and  $H_2$  through a discharge source, measured using 3.495 eV photon energy, is dominated by a detachment transition that is consistent with the  $OH^-$ -isoprene IMC. Autodetachment signal is observed

when the photon energy is tuned through the \*OH·isoprene + e<sup>-</sup> photodetachment threshold. The e<sup>-</sup>KEs of the autodetachment features are independent of the photon energy over a ca. 0.3 eV range, suggesting that the autodetaching anion is not a vibrationally excited OH<sup>-</sup>·isoprene. A viable explanation supported by computational results is that, near the \*OH·isoprene + e<sup>-</sup> threshold, the radical van der Waals complex may undergo an H-abstraction reaction, weakly trapping the threshold electron in a temporary dipole-bound state of the reaction complex. This state then undergoes vibrational autodetachment of the electron with e<sup>-</sup>KEs that encode the low-frequency modes of the transient complex.

Additional signal in the PE spectrum observed at lower e<sup>-</sup>BEs are assigned to the ensemble of HO-isoprene adduct MIs and alkenoxide ions sharing m/z 85. The signal observed exclusively in the PE spectrum collected using 3.495 eV photon energy at higher e<sup>-</sup>BE (0.5  $\leq$  e<sup>-</sup>KE  $\leq$  0.9 eV) is tentatively assigned to a resonance with the lowest energy temporary anion state of isoprene. Subtle enhancement was observed in the same range of e<sup>-</sup>KE values in the PE spectrum of the O<sub>2</sub>-isoprene IMC.

# ASSOCIATED CONTENT

# Supporting Information

The Supporting Information is available free of charge at https://pubs.acs.org/doi/10.1021/acs.jpca.0c01250.

Relative energies of the various  $C_4H_5O_2$  anion conformational isomers and their predicted VDE values at MP2/ma-def2-TZVP(-f) and IP-EOM-CCSD/aug-cc-pVTZ; CAM-B3LYP/aug-cc-pVTZ relative energies, ADEs, and VDE values; optimized geometries at CAM-B3LYP/aug-cc-pVTZ and MP2/ma-def2-TZVP(-f); and simulation parameters (PDF)

# AUTHOR INFORMATION

#### **Corresponding Authors**

Thomas Sommerfeld — Department of Chemistry and Physics, Southeast Louisiana University, Hammond, Louisiana 70402, United States; orcid.org/0000-0001-8105-5414; Email: thomas.sommerfeld@selu.edu; Fax: (985) 549-5126 Caroline Chick Jarrold — Department of Chemistry, Indiana University, Bloomington, Indiana 47405, United States; orcid.org/0000-0001-9725-4581; Phone: (812) 856-1190; Email: cjarrold@indiana.edu; Fax: (812) 855-8300

#### **Authors**

Marissa A. Dobulis — Department of Chemistry, Indiana University, Bloomington, Indiana 47405, United States Michael C. Thompson — Department of Chemistry, Indiana University, Bloomington, Indiana 47405, United States Kellyn M. Patros — Department of Chemistry, Indiana University, Bloomington, Indiana 47405, United States

Complete contact information is available at: https://pubs.acs.org/10.1021/acs.jpca.0c01250

## **Author Contributions**

\*M. A. Dobulis and M. C. Thompson are co first authors.

Notes

The authors declare no competing financial interest.

## ACKNOWLEDGMENTS

C.C.J. gratefully acknowledges the National Science Foundation, Grant No. CHE-1664965, for their generous support. T.S. gratefully acknowledges support by the National Science Foundation, Grant No. CHE-1565495.

## REFERENCES

- (1) Guenther, A. B.; Jiang, X.; Heald, C. L.; Sakulyanontvittaya, T.; Duhl, T.; Emmons, L. K.; Wang, X. The Model of Emissions of Gases and Aerosols from Nature Version 2.1 (MEGAN2.1): An Extended and Updated Framework for Modeling Biogenic Emissions. *Geosci. Model Dev.* 2012, 5, 1471–1492.
- (2) Gligorovski, S.; Strekowski, R.; Barbati, S.; Vione, D. Environmental Implications of Hydroxyl Radicals (·OH). *Chem. Rev.* **2015**, *115*, 13051–13092.
- (3) Jaeglé, L.; Jacob, D. J.; Brune, W. H.; Wennberg, P. O. Chemistry of  ${\rm HO_x}$  Radicals in the Upper Troposphere. *Atmos. Environ.* **2001**, 35, 469–489.
- (4) Wennberg, P. O.; Hanisco, T. F.; Jaeglé, L.; Jacob, D. J.; Hintsa, E. J.; Lanzendorf, E. J.; Anderson, J. G.; Gao, R.-S.; Keim, E. R.; Donnelly, S. G.; et al. Hydrogen Radicals, Nitrogen Radicals, and the Production of  $O_3$  in the Upper Troposphere. *Science* **1998**, 279, 49–53.
- (5) Atkinson, R. Kinetics and Mechanisms of the Gas-Phase Reactions of the Hydroxyl Radical with Organic Compounds Under Atmospheric Conditions. *Chem. Rev.* **1986**, *86*, 69–201.
- (6) Perry, R. A.; Atkinson, R.; Pitts, J. N. Kinetics and Mechanism of the Gas Phase Reaction of Hydroxyl Radicals with Aromatic Hydrocarbons over the Temperature Range 296–473 K. *J. Phys. Chem.* **1977**, *81*, 296–304.
- (7) Stevens, P.; L'Esperance, D.; Chuong, B.; Martin, G. Measurements of the Kinetics of the OH-Initiated Oxidation of Isoprene: Radical Propagation in the OH + Isoprene + O<sub>2</sub> + NO Reaction System. *Int. J. Chem. Kinet.* **1999**, *31*, 637–643.
- (8) Tully, F. P.; Ravishankara, A. R.; Thompson, R. L.; Nicovich, J. M.; Shah, R. C.; Kreutter, N. M. Kinetics of the Reactions of Hydroxyl Radical with Benzene and Toluene. *J. Phys. Chem.* **1981**, 85, 2262–2269
- (9) Dillon, T. J.; Dulitz, K.; Groß, C. B. M.; Crowley, J. N. Temperature-Dependent Rate Coefficients for the Reactions of the Hydroxyl Radical with the Atmospheric Biogenics Isoprene, alphapinene and delta-3-carene. *Atmos. Chem. Phys.* **2017**, *17*, 15137–15150.
- (10) Khaled, F.; Giri, B. R.; Liu, D.; Assaf, E.; Fittschen, C.; Farooq, A. Insights into the Reactions of Hydroxyl Radical with Diolefins from Atmospheric to Combustion Environments. *J. Phys. Chem. A* **2019**, 123, 2261–2271.
- (11) Chuong, B.; Stevens, P. S. Kinetic Study of the OH + Isoprene and OH + Ethylene Reactions between 2 and 6 Torr and over the Temperature Range 300–423 K. *J. Phys. Chem. A* **2000**, *104*, 5230–5237.
- (12) Lee, W.; Stevens, P. S.; Hites, R. A. Rate Constants for the Gas-Phase Reactions of Methylphenanthrenes with OH as a Function of Temperature. *J. Phys. Chem. A* **2003**, *107*, 6603–6608.
- (13) Stevens, P. S.; Seymour, E.; Li, Z. Theoretical and Experimental Studies of the Reaction of OH with Isoprene. *J. Phys. Chem. A* **2000**, 104, 5989–5997
- (14) Morales-Roque, J.; Carrillo-Cárdenas, M.; Jayanthi, N.; Cruz, J.; Pandiyan, T. Theoretical and Experimental Interpretations of Phenol Oxidation by the Hydroxyl Radical. *J. Mol. Struct.: THEOCHEM* **2009**, *910*, 74–79.
- (15) Shiroudi, A.; Deleuze, M. S.; Canneaux, S. Theoretical Study of the Oxidation Mechanisms of Naphthalene Initiated by Hydroxyl Radicals: The OH-Addition Pathway. *J. Phys. Chem. A* **2014**, *118*, 4593–4610.
- (16) Shiroudi, A.; Deleuze, M. S. Theoretical Study of the Oxidation Mechanisms of Naphthalene Initiated by Hydroxyl Radicals: The H Abstraction Pathway. *J. Phys. Chem. A* **2014**, *118*, 3625–3636.

- (17) Krasnoperov, L. N.; Butkovskaya, N.; Le Bras, G. Branching Ratios in the Hydroxyl Reaction with Propene. *J. Phys. Chem. A* **2011**, *115*, 2498–2508.
- (18) Greenwald, E. E.; North, S. W.; Georgievskii, Y.; Klippenstein, S. J. A Two Transition State Model for Radical—Molecule Reactions: Applications to Isomeric Branching in the OH—Isoprene Reaction. *J. Phys. Chem. A* **2007**, *111*, 5582—5592.
- (19) Peeters, J.; Nguyen, T. L.; Vereecken, L. HO<sub>x</sub> Radical Regeneration in the Oxidation of Isoprene. *Phys. Chem. Chem. Phys.* **2009**, *11*, 5935–5939.
- (20) Tully, F. P.; Goldsmith, J. E. M. Kinetic Study of the Hydroxyl Radical-Propene Reaction. *Chem. Phys. Lett.* **1985**, *116*, 345–352.
- (21) Zádor, J.; Jasper, A. W.; Miller, J. A. The Reaction Between Propene and Hydroxyl. *Phys. Chem. Chem. Phys.* **2009**, *11*, 11040–11053
- (22) Jeon, J.; Barker, J. R.; Song, K. OH + Isoprene: A Direct Dynamics Study. *Bull. Korean Chem. Soc.* **2017**, 38, 651–660.
- (23) Wennberg, P. O.; Bates, K. H.; Crounse, J. D.; Dodson, L. G.; McVay, R. C.; Mertens, L. A.; Nguyen, T. B.; Praske, E.; Schwantes, R. H.; Smarte, M. D.; et al. Gas-Phase Reactions of Isoprene and Its Major Oxidation Products. *Chem. Rev.* **2018**, *118*, 3337–3390.
- (24) Zhang, Y.; Chao, K.; Sun, J.; Su, Z.; Pan, X.; Zhang, J.; Wang, R. Theoretical Study on the Gas Phase Reaction of Allyl Alcohol with Hydroxyl Radical. *J. Phys. Chem. A* **2013**, *117*, 6629–6640.
- (25) Zhang, Y.; Chao, K.; Sun, J.; Zhang, W.; Shi, H.; Yao, C.; Su, Z.; Pan, X.; Zhang, J.; Wang, R. Theoretical Study on the Gas Phase Reaction of Allyl Chloride with Hydroxyl Radical. *J. Chem. Phys.* **2014**, *140*, No. 084309.
- (26) Zhang, Y.; Sun, J.; Chao, K.; Sun, H.; Wang, F.; Tang, S.; Pan, X.; Zhang, J.; Wang, R. Mechanistic and Kinetic Study of CF<sub>3</sub>CH=CH<sub>2</sub> + OH Reaction. *J. Phys. Chem. A* **2012**, *116*, 3172–3181.
- (27) Zhang, Y.; Sun, J.; Zhang, W.; Tang, Y.; Wang, R. Theoretical Study on the Gas Phase Reaction of Propargyl Alcohol with Hydroxyl Radical. *J. Comput. Chem.* **2014**, *35*, 1646–1656.
- (28) Allodi, M. A.; Kirschner, K. N.; Shields, G. C. Thermodynamics of the Hydroxyl Radical Addition to Isoprene. *J. Phys. Chem. A* **2008**, 112, 7064–7071.
- (29) Benitez, Y.; Lu, D.; Lunny, K. G.; Li, J.; Guo, H.; Continetti, R. E. Photoelectron—Photofragment Coincidence Studies on the Dissociation Dynamics of the OH—CH<sub>4</sub> Complex. *J. Phys. Chem. A* **2019**, *123*, 4825—4833.
- (30) Patros, K. M.; Mann, J. E.; Jarrold, C. C. Photoelectron Imaging Spectra of O<sub>2</sub>-VOC and O<sub>4</sub>-VOC Complexes. *J. Phys. Chem. A* **2016**, 120, 7828–7838.
- (31) Patros, K. M.; Mann, J. E.; Jarrold, C. C. O<sub>2</sub>-·[Polar VOC] Complexes: H-bonding versus Charge-Dipole Interactions, and the Noninnocence of Formaldehyde. *J. Phys. Chem. A* **2017**, *121*, 5459–5467.
- (32) Patros, K. M.; Mann, J. E.; Dobulis, M. A.; Thompson, M. C.; Jarrold, C. C. Probing Alkenoxy Radical Electronic Structure Using Anion PEI Spectroscopy. *J. Chem. Phys.* **2019**, *150*, No. 034302.
- (33) Mann, J. E.; Troyer, M. E.; Jarrold, C. C. Photoelectron Imaging and Photodissociation of Ozonide in  $O_3^-\cdot (O_2)_n$  (n=1-4) Clusters. *J. Chem. Phys.* **2015**, *142*, 124305.
- (34) Oliveira, A. M.; Lehman, J. H.; McCoy, A. B.; Lineberger, W. C. Photoelectron Spectroscopy of the Hydroxymethoxide Anion, H<sub>2</sub>C-(OH)O<sup>-</sup>. *J. Chem. Phys.* **2016**, *145* (12), 124317.
- (35) Duncan, M. A. Infrared Laser Spectroscopy of Mass-Selected Carbocations. J. Phys. Chem. A 2012, 116, 11477-11491.
- (36) Posey, L. A.; Deluca, M. J.; Johnson, M. A. Demonstration of a Pulsed Photoelectron Spectrometer on Mass-Selected Negative Ions: O<sup>-</sup>, O<sub>2</sub><sup>-</sup>, and O<sub>4</sub><sup>-</sup>. *Chem. Phys. Lett.* **1986**, *131*, 170–174.
- (37) Bakker, J. M. B. A Beam-Modulated Time-of-Flight Mass Spectrometer. I. Theoretical Considerations. *J. Phys. E: Sci. Instrum.* **1973**, *6*, 785–789.
- (38) Bakker, J. M. B. A Beam-Modulated Time-of-Flight Mass Spectrometer. II. Experimental Work. *J. Phys. E: Sci. Instrum.* **1974**, *7*, 364–368.

- (39) Eppink, A. T. J. B.; Parker, D. H. Velocity Map Imaging of Ions and Electrons Using Electrostatic Lenses: Application in Photoelectron and Photofragment Ion Imaging of Molecular Oxygen. *Rev. Sci. Instrum.* 1997, 68, 3477–3484.
- (40) Doyle, M. B.; Abeyasera, C.; Suits, A. G. NuAcq 0.9: Native Megapixel Ion Imaging with Centroiding to 4 Mpix Using Inexpensive USB-2 Cameras. Available at faculty.missouri.edu/suitsa/NuAqc.html.
- (41) Dribinski, V.; Ossadtchi, A.; Mandelshtam, V. A.; Reisler, H. Reconstruction of Abel-Transformable Images: The Gaussian Basis-Set Expansion Abel Transform Method. *Rev. Sci. Instrum.* **2002**, *73*, 2634–2642.
- (42) Ervin, K. M.; Anusiewicz, I.; Skurski, P.; Simons, J.; Lineberger, W. C. The Only Stable State of  ${\rm O_2}^-$  Is the X  $^2\Pi_{\rm g}$  Ground State and It (Still!) Has an Adiabatic Electron Detachment Energy of 0.45 eV. *J. Phys. Chem. A* **2003**, *107*, 8521–8529.
- (43) Kendall, R. A.; D, T. H., Jr.; Harrison, R. J. Electron Affinities of the First-Row Atoms Revisited. Systematic Basis Sets and Wave Functions. *J. Chem. Phys.* **1992**, *96*, 6796–6806.
- (44) Zheng, J.; Xu, X.; Truhlar, D. G. Minimally Augmented Karlsruhe Basis Sets. *Theor. Chem. Acc.* **2011**, *128*, 295–305.
- (45) Raghavachari, K.; Trucks, G. W.; Pople, J. A.; Head-Gordon, M. A Fifth-Order Perturbation Comparison of Electron Correlation Theories. *Chem. Phys. Lett.* **1989**, *157*, 479–483.
- (46) Riplinger, C.; Neese, F. An Efficient and Near Linear Scaling Pair Natural Orbital Based Local Coupled Cluster Method. *J. Chem. Phys.* **2013**, *138*, No. 034106.
- (47) Riplinger, C.; Pinski, P.; Becker, U.; Valeev, E. F.; Neese, F. Sparse Maps—A Systematic Infrastructure for Reduced-Scaling Electronic Structure Methods. II. Linear Scaling Domain Based Pair Natural Orbital Coupled Cluster Theory. *J. Chem. Phys.* **2016**, *144*, No. 024109.
- (48) Riplinger, C.; Sandhoefer, B.; Hansen, A.; Neese, F. Natural Triple Excitations in Local Coupled Cluster Calculations with Pair Natural Orbitals. *J. Chem. Phys.* **2013**, *139*, 134101.
- (49) Stanton, J. F.; Gauss, J. Analytic Energy Derivatives for Ionized States Described by the Equation-of-Motion Coupled Cluster Method. *J. Chem. Phys.* **1994**, *101*, 8938.
- (50) Stanton, J. F.; Gauss, J. A Simple Scheme for the Direct Calculation of Ionization Potentials with Coupled-Cluster Theory that Exploits Established Excitation Energy Methods. *J. Chem. Phys.* 1999, 111, 8785.
- (51) Neese, F. The ORCA Program System. Wiley Interdiscip. Rev.: Comput. Mol. Sci. 2012, 2, 73–78.
- (52) Neese, F. Software Update: The ORCA Program System, Version 4.0. Wiley Interdiscip. Rev.: Comput. Mol. Sci. 2018, 8, No. e1327.
- (53) Yanai, T.; Tew, D. P.; Handy, N. C. A New Hybrid Exchange—Correlation Functional Using the Coulomb-Attenuating Method (CAM-B3LYP). *Chem. Phys. Lett.* **2004**, 393, 51–57.
- (54) Frisch, M. J.; Trucks, G. W.; Schlegel, H. B.; Scuseria, G. E.; Robb, M. A.; Cheeseman, J. R.; Scalmani, G.; Barone, V.; Petersson, G. A.; Nakatsuji, H.; et al. *Gaussian 09*, Revision D.01; Gaussian, Inc.: Wallingford, CT, USA, 2009.
- (55) Frisch, M. J.; Trucks, G. W.; Schlegel, H. B.; Scuseria, G. E.; Robb, M. A.; Cheeseman, J. R.; Scalmani, G.; Barone, V.; B. Mennucci, G. A.; Petersson, G. A.; et al. *Gaussian 16*, Rev. C.01; Gaussian, Inc.: Wallingford, CT, USA, 2016.
- (56) Schaugaard, R. N.; Topolski, J. E.; Ray, M.; Raghavachari, K.; Jarrold, C. C. Insight into Ethylene Interactions with Molybdenum Suboxide Cluster Anions from Photoelectron Spectra of Chemifragments. J. Chem. Phys. 2018, 148, No. 054308.
- (57) Smith, J. R.; Kim, J. B.; Lineberger, W. C. High-Resolution Threshold Photodetachment Spectroscopy of OH<sup>-</sup>. *Phys. Rev. A: At., Mol., Opt. Phys.* **1997**, *55*, 2036.
- (58) Schulz, P. A.; Mead, R. D.; Jones, P. L.; Lineberger, W. C. OH-and OD-Threshold Photodetachment. J. Chem. Phys. 1982, 77, 1153.
- (59) Lyle, J.; Jagau, T.-C.; Mabbs, R. Spectroscopy of Temporary Anion States: Renner-Teller Coupling and Electronic Autodetach-

- ment in Copper Difluoride Anion. Faraday Discuss. 2019, 217, 533-546.
- (60) Lyle, J.; Wedig, O.; Gulania, S.; Krylov, A. I.; Mabbs, R. Channel Branching Ratios in CH<sub>2</sub>CN- Photodetachment: Rotational Structure and Vibrational Energy Redistribution in Autodetachment. *J. Chem. Phys.* **2017**, *147*, 234309.
- (61) Jagau, T.-C.; Dao, D. B.; Holtgrewe, N. S.; Krylov, A. I.; Mabbs, R. Same but Different: Dipole-Stabilized Shape Resonances in CuF<sup>-</sup> and AgF<sup>-</sup>. *J. Phys. Chem. Lett.* **2015**, *6*, 2786–2793.
- (62) Czekner, J.; Cheung, L. F.; Kocheril, G. S.; Wang, L. S. Probing the Coupling of a Dipole-Bound Electron with the Molecular Core. *Chem. Sci.* **2019**, *10*, 1386–1391.
- (63) Zhu, G. Z.; Qian, C. H.; Wang, L. S. Dipole-Bound Excited States and Resonant Photoelectron Imaging of Phenoxide and Thiophenoxide Anions. *J. Chem. Phys.* **2018**, *149*, 164301.
- (64) Zhu, G. Z.; Liu, Y.; Wang, L. S. Observation of Excited Quadrupole-Bound States in Cold Anions. *Phys. Rev. Lett.* **2017**, *119*, No. 023002.
- (65) Belogolova, E. F.; Liu, G.; Doronina, E. P.; Ciborowski, S. M.; Sidorkin, V. F.; Bowen, K. H. Dipole-Bound Anions of Intramolecular Complexes. *J. Phys. Chem. Lett.* **2018**, *9*, 1284–1289.
- (66) Liu, G.; Ciborowski, S. M.; Pitts, C. R.; Graham, J. D.; Buytendyk, A. M.; Lectka, T.; Bowen, K. H. Observation of the Dipole- and Quadrupole-Bound Anions of 1,4-Dicyanocyclohexane. *Phys. Chem. Phys.* **2019**, *21*, 18310–18315.
- (67) Yokoyama, K.; Leach, G. W.; Kim, J. B.; Lineberger, W. C. Autodetachment Spectroscopy and Dynamics of Dipole Bound States of Negative Ions: <sup>2</sup>A<sub>1</sub>-<sup>2</sup>B<sub>1</sub> transitions of H<sub>2</sub>CCC<sup>-</sup>. *J. Chem. Phys.* **1996**, 105, 10696–10705.
- (68) Lykke, K. R.; Neumark, D. M.; Andersen, T.; Trapa, V. J.; Lineberger, W. C. Autodetachment Spectroscopy and Dynamics of CH<sub>2</sub>CN<sup>--</sup> and CD<sub>2</sub>CN<sup>--</sup>. *J. Chem. Phys.* **1987**, *87*, 6842–6853.
- (69) Neumark, D. M.; Lykke, K. R.; Andersen, T.; Lineberger, W. C. Infrared-Spectrum and Autodetachment Dynamics of NH<sup>-</sup>. *J. Chem. Phys.* **1985**, 83, 4364–4373.
- (70) Andersen, T.; Lykke, K. R.; Neumark, D. M.; Lineberger, W. C. Autodetachment Study of the Electronic Spectroscopy of FeO<sup>-</sup>. *J. Chem. Phys.* **1987**, *86*, 1858–1867.
- (71) Lykke, K. R.; Murray, K. K.; Neumark, D. M.; Lineberger, W. C. High-Resolution Studies of Autodetachment in Negative Ions. *Philos. Trans. R. Soc. London A* **1988**, 324, 179–196.
- (72) Jordan, K. D.; Wang, F. Theory of Dipole-Bound Anions. *Annu. Rev. Phys. Chem.* **2003**, *54*, 367–396.
- (73) Hammer, N. I.; Diri, K.; Jordan, K. D.; Desfrancois, C.; Compton, R. N. Dipole-Bound Anions of Carbonyl, Nitrile, and Sulfoxide Containing Molecules. *J. Chem. Phys.* **2003**, *119*, 3650–
- (74) Tsai, M.-K.; Wang, F.; Jordan, K. D. Electron Attachment to (H<sub>2</sub>O)<sub>2</sub>Ar<sub>n</sub> Clusters. *J. Phys. Chem. A* **2004**, *108*, 2912–2921.
- (75) Allan, M.; Asmis, K. R.; Popovic, D. B.; Stepanovic, M.; Mason, N. J.; Davies, J. A. Production of Vibrationally Autodetaching  $O_2$  in Low-Energy Electron Impact on Ozone. J. Phys. B: At., Mol. Opt. Phys. 1996, 29, 3487–3495.
- (76) Čížek, M.; Horácek, J.; Allen, M.; Fabrikant, I. I.; Domcke, W. Vibrational Excitation of Hydrogen Fluoride by Low-Energy Electrons: Theory and Experiment. *J. Phys. B: At., Mol. Opt. Phys.* **2003**, *36*, 2837–2849.
- (77) Allan, M.; Čížek, M.; Horácek, J.; Domcke, W. Electron Scattering in Cooled HCl: Boomerang Structures and Outer-Well Resonances in Elastic and Vibrational Excitation Cross Sections. *J. Phys. B: At., Mol. Opt. Phys.* **2000**, 33, L209.
- (78) Zawadzki, M.; Čížek, M.; Houfek, K.; Čurík, R.; Ferus, M.; Civiš, S.; Kočiš, J.; Fedor, J. Resonances and Dissociative Electron Attachment in HNCO. *Phys. Rev. Lett.* **2018**, *121*, 143402.
- (79) Jordan, K. D.; Burrow, P. D. Temporary Anion States of Polyatomic Hydrocarbons. *Chem. Rev.* **1987**, *87*, 557–588.